OPTICA

Hyperentanglement quantum communication over a 50 km noisy fiber channel

Zhen-Qiu Zhong,[1,2,3] Xiao-Hai Zhan,[1,2,3] Jia-Lin Chen,[1,2,3] Shuang Wang,[1,2,3,*] Zhen-Qiang Yin,[1,2,3] Jia-Qi Geng,[1,2,3] De-Yong He,[1,2,3,4] Wei Chen,[1,2,3,4] Guang-Can Guo,[1,2,3,4] and Zheng-Fu Han[1,2,3,4]

[1]CAS Key Laboratory of Quantum Information, University of Science and Technology of China, Hefei 230026, China
[2]Anhui Province Key Laboratory of Quantum Network, University of Science and Technology of China, Hefei 230026, China
[3]CAS Center for Excellence in Quantum Information and Quantum Physics, University of Science and Technology of China, Hefei 230026, China
[4]Hefei National Laboratory, University of Science and Technology of China, Hefei 230088, China
*wshuang@ustc.edu.cn

Received 15 March 2024; revised 4 June 2024; accepted 24 June 2024; published 25 July 2024

High-dimensional entanglement not only offers a high security level for quantum communication but also promises improved information capacity and noise resistance of the system. However, due to various constraints on different high-dimensional degrees of freedom, whether these advantages can bring improvement to the actual implementation is still not well proven. Here we present a scheme to fully utilize these advantages over long-distance noisy fiber channels. We exploit polarization and time-bin hyperentanglement to achieve high-dimensional coding, and observe significant enhancements in secure key rates and noise tolerance that surpass the capabilities of qubit systems. Moreover, the demonstration achieves a distribution up to 50 km, which is the longest distance for high-dimensional entanglement-based quantum key distribution up to date, to our knowledge. Our demonstration validates the potential of high-dimensional entanglement for quantum communications over long-distance noisy channels, paving the way for a resilient and resource-efficient quantum network.

https://doi.org/10.1364/OPTICA.523955

1. INTRODUCTION

Quantum communication is one of the most mature areas of quantum technology, and its implementation is crucial for the construction of a global-scale quantum internet. Quantum key distribution (QKD) [1–3] is the most prominent example of quantum communication that enables distant parties to share secure keys. Unlike classical cryptography, its security is guaranteed by fundamental laws of physics [4–6] rather than the computational hardness assumptions. However, in practical implementations, the security also relies on the trust in quantum state sources and measurement devices [7]. Although the trust assumptions may seem reasonable, they can potentially create loopholes for eavesdroppers to exploit. Fortunately, entanglement-based QKD can relinquish trust in the source or even all quantum devices, thus providing a higher level of practical security [8–12]. At the same time, entanglement allows fully connected multi-user network architectures [13–16], which is an ideal candidate for future quantum networks. Over the past decade, the practical potential of entanglement-based QKD has been realized in laboratories and various real-world environments [17–21].

Nevertheless, there are still two fundamental challenges in practical implementation: the relatively low key rate and the high susceptibility to noise. First, the quantum signals are very weak and cannot be cloned or amplified, meaning that only a meager number of photons can be used to generate the key after a long-distance transmission. Additionally, for a two-dimensional system, each surviving photon can only carry 1 bit of information, thus the achievable key rate is limited. Second, the quantum system is inherently vulnerable and can be easily compromised by any interactions with the environment or the presence of noise [22,23]. Once the noise level reaches a certain threshold, it is no longer possible to share any secure keys. Furthermore, the difficulty lies in the fact that in practical systems, noise can arise from diverse sources, including stray light, various scatterings in channels, or even from eavesdropping attacks [19,24,25]. These noises are challenging to suppress effectively, which severely constrains the usage of QKD. Fortunately, high-dimensional entanglement is a natural and good carrier for these challenges. In theory, high-dimensional coding offers two key advantages: increased information capacity and superior noise tolerance [26,27]. In ideal conditions, a d-dimensional quantum state can encode up to $\log_2 d$ bits of information, which ensures the potential for higher key rates in QKD [28–31]. At the same time, as the dimension increases, high-dimensional systems exhibit excellent noise tolerance [32–35], whether it be environmental or resulting from eavesdropping attacks.

The benefits of high information capacity have been demonstrated in various experiments [36–39]. Recently, with the advancement of space encoding technology, these demonstrations have become even more diverse [40,41]. However, exploiting the high noise resistance in practical QKD experiments remains a challenging task. This is partly because high-dimensional entangled systems are often more complex, and achieving high-fidelity state preparation [39,42], manipulation [43,44], and distribution [45–47] can be challenging. Furthermore, the complexity of the system may introduce additional noise and cost more keys for error correction, potentially diminishing the actual noise resistance advantages. To fully leverage the advantages of high-dimensional entanglement in noisy QKD, a simultaneous subspace coding protocol is proposed [48]. This scheme allows the flexible subspace dimensions settings to achieve an optimal balance between information capacity and error correction costs. Importantly, this trade-off guarantees adaptability to changing noise conditions, which has also been demonstrated by recent experiments in free-space links [49,50]. However, the application scenarios for free-space links are highly dependent on the meteorological conditions, which poses a significant challenge to their potential. In contrast, a fiber channel presents another attractive option as it is less susceptible to weather disturbances and can provide a more stable operation. The noise is primarily caused by cross-talk or various scattering effects of co-propagating signals, rather than the environment. Unfortunately, due to various limitations of different degrees of freedom (DOFs), the task of high-dimensional entanglement-based QKD over long-distance noisy fiber channels is not easy. To date, no experimental demonstration has yet fully illustrated the benefits of high-dimensional entanglement in these scenarios.

In this work, we fully demonstrate the practical enhancement of high-dimensional entanglement to quantum communication systems over a 50 km noisy fiber channel. This is also the longest experimental implementation of high-dimensional entanglement-based QKD to date. We take full use of the high information capacity and high noise resilience of high-dimensional entanglement through the flexible subspace dimension setting [48]. The experimental results show that, even after a long-distance distribution, a secure key rate exceeding 1 bit per sifted signal can be obtained in low-noise environments and a positive secure key can be established at extreme noise levels where qubit systems are not viable. In addition, we project a practical application scenario where quantum signals and classical signals coexist in the same fiber. We have successfully achieved coexistence with equivalent optical power for at least six 10 Gbps classical communication channels without the need for additional filters, while narrow passband filters are typically required for qubit systems [51]. Our scheme enables the optimal utilization of high-dimensional entanglement in practical scenarios, paving the way for constructing a noise-robust and resource-efficient quantum internet.

2. HIGH-DIMENSIONAL ENTANGLEMENT SUBSPACE CODING PROTOCOL

First, let us start with the basic working principle of the high-dimensional entanglement-based QKD protocol developed in [48]. In the protocol, a source distributes a $d \times d$ entangled state $\rho_{AB} \in \mathcal{H}_A \otimes \mathcal{H}_B$ to the communicating parties, Alice and Bob. Then they each randomly choose the computational basis or the mutually unbiased basis in subspace (subspace Fourier-transform basis) to perform a measurement of the photon they received. Here, the subspace is split from the total d-dimensional Hilbert space. If the subspace-dimension choice is k, then the number of subspaces is d/k. Both parties need to record the outcomes x and the sequence number m of the subspace. After repeating the above steps for N rounds, Alice and Bob sift out the events with the same basis choice and subspace number. Finally, they should perform parameter estimation and post-processing steps in each subspace and extract the secure key. Note that these processes are carried out separately in each subspace. For each k-dimensional subspace $H^k_{A,m} \otimes \mathcal{H}^k_{B,m}$ (m is the sequence number of the subspace), the asymptotic key rate per sifted signal can be estimated as

$$K_m \geq \log_2(k) - H(\delta_c) - H(\delta_f), \tag{1}$$

where δ_c and δ_f are the error rate in computational-basis and Fourier-basis, which can be calculated based on the detection results; and $H(x) = -(1-x)\log_2(1-x) - x\log_2[x/(k-1)]$ is the k-dimensional Shannon entropy. Sifted signals represent the valid coincidence events where Alice and Bob have the same basis choice and subspace number. The total asymptotic key rate per second for a d-dimensional system K_{tot} can be calculated by

$$K_{\text{tot}} \geq \sum_{m=0}^{d/k-1} N_m K_m, \tag{2}$$

where N_m is the number of sifted signals per second in subspace m. The key rate per sifted signal K_{pss} can in turn be calculated by dividing K_{tot} by the total number of the sifted signals per second N_{tot}, i.e., $K_{pss} = K_{\text{tot}}/N_{\text{tot}}$.

3. EXPERIMENTAL IMPLEMENTATION

In our experiment, we use a time-bin and polarization hyper-entangled state [see Figs. 1(a)] as the state ρ_{AB} required in the protocol. To generate such entangled photon pairs, we use an asymmetric Faraday-Michelson interferometer (FMI) to split each pulse emitted from the laser into two time-bins separated by $\tau = 5$ ns. The double pulses are then amplified and frequency doubled to pump a periodically poled potassium titanyl phosphate (PPKTP) crystal (poling period of 46.2 μm) inside a polarizing Sagnac interferometer [52,53]. The resulting quantum state features both time-bin and polarization entanglement and can be written as $|\Psi_{AB}\rangle = \frac{1}{2}(|HV\rangle + |VH\rangle) \otimes (|t_0 t_0\rangle + |t_1 t_1\rangle)$, where H (V) indicates the horizontal (vertical) polarization state, and t_0 (t_1) represents the early (late) time-bin. If we encode $|Ht_0\rangle_A$, $|Vt_0\rangle_B$ as $|0\rangle$, $|Ht_1\rangle_A$, $|Vt_1\rangle_B$ as $|1\rangle$, $|Vt_0\rangle_A$, $|Ht_0\rangle_B$ as $|2\rangle$, and $|Vt_1\rangle_A$, $|Ht_1\rangle_B$ as $|3\rangle$, then we get

$$|\Psi_{AB}\rangle = \frac{1}{2}(|00\rangle + |11\rangle + |22\rangle + |33\rangle). \tag{3}$$

The outputs of the entangled photon source are coupled into single-mode fibers through couplers, and then multiplexed into the fiber channels through CH35 of the International Telecommunication Union (ITU) DWDM grid. At the same time, a continuous-wave laser at 1530 nm is also multiplexed into the fiber channel to generate noise by means of Raman scattering.

Both Alice's and Bob's sides [see Figs. 1(a)–1(c)] are equipped with an all-fiber setup to perform measurements in two mutually

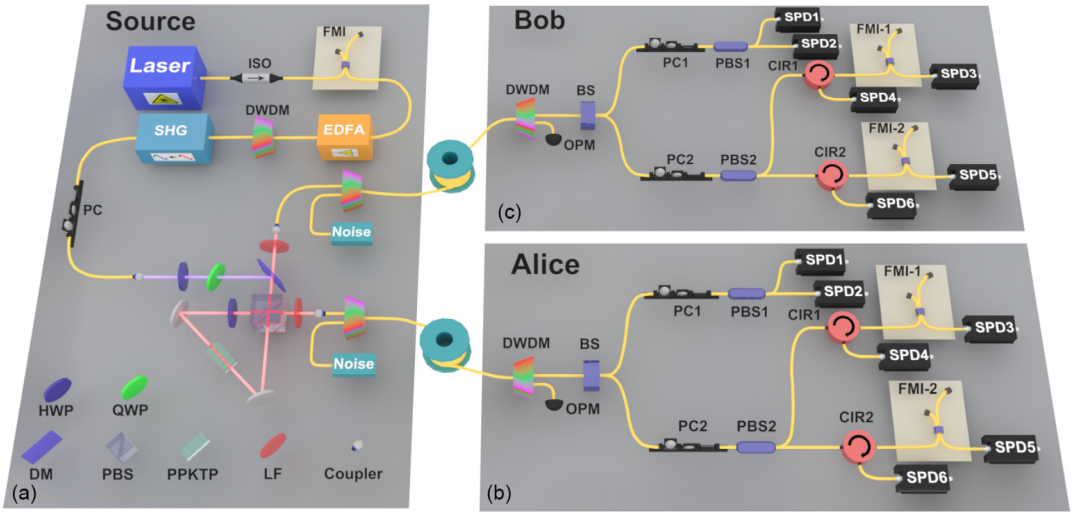

Fig. 1. Experimental setup. (a) Preparation of the 4D entanglement source. A semiconductor gain-switched laser generates optical pulses with a center wavelength of 1549.32 nm, a pulse width of 200 ps, and a repetition rate of 50 MHz. The pulse is then amplified by the erbium-doped fiber amplifier (EDFA) after passing through the optical isolator (ISO) and a FMI with a 1 m arm length difference. The dense wavelength-division multiplexing (DWDM, with 100 GHz spacing) is used to filter out the noise introduced by the EDFA during amplification. A homemade frequency doubling module converts the wavelength to 774.66 nm via second-harmonic generation (SHG). The PC is the polarization controller that is used to rotate the polarization of the light beam emitting from the coupler to the horizontal. Then, the light beam is injected into a Sagnac interferometer [52,53] to pump a type-II PPKTP crystal and generates a two-photon state $1/2(|HV\rangle + |VH\rangle) \otimes (|t_0 t_0\rangle + |t_1 t_1\rangle)$. Finally, after passing through the long-pass filter (LF), the entangled photon pairs are multiplexed into the fiber channel by DWDM (with 100 GHz spacing). In addition, a CW laser with a central wavelength of 1530 nm is multiplexed into the channels to introduce noise. (b), (c) Alice's and Bob's measurement setups for the 4D system. Each user was interconnected with the entanglement source via a spool of fiber. We executed our experiments at three distinct distances: 2 × 0 km, 2 × 10 km, and 2 × 25 km. Each measurement setup is an all-fiber structure, which consists of DWDM, optical power meter (OPM), PCs, polarization beam splitters (PBSs), beam splitter (BS), circulators (CIRs), FMIs, and single-photon detectors (SPDs). Before the measurement, a DWDM is used to demultiplex the classical laser and quantum signals. The classical laser is detected by OPM, while quantum signals are sent for measurements with two bases. The photon detection events are recorded by single-photon avalanche diodes, which are operated in gated Geiger mode. All FMIs are placed in insulated boxes with an accuracy of approximately 10 μm in the arm length difference. In addition, a fiber phase shifter is installed in both FMIs on Bob's side to align the phase between Alice, Bob, and the source.

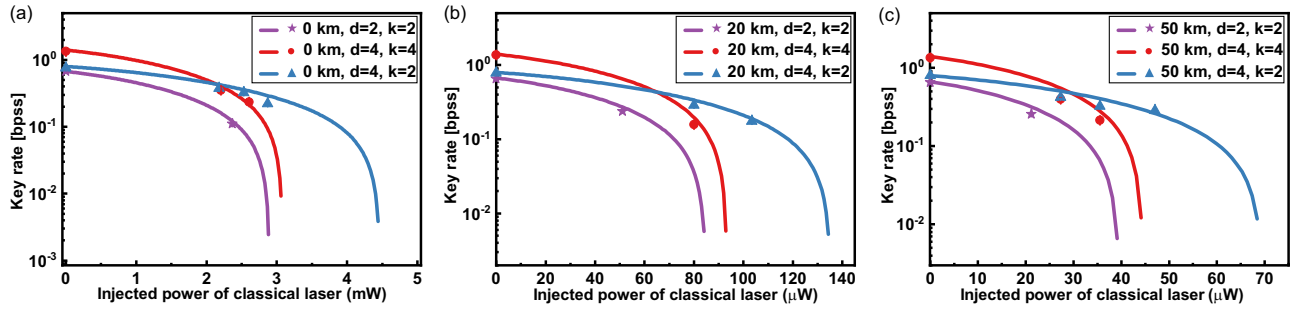

Fig. 2. Key rate of bits per sifted signal (bpss) versus the injected classical laser power over (a) 0 km, (b) 20 km, and (c) 50 km. The solid lines in the figure are the simulation results, and the discrete points are the experimental results. Experimental error bars indicate one standard deviation and are obtained assuming Poisson detection statistics. The error bars for the key rate are inside the symbols.

unbiased bases: the computational basis and the subspace Fourier-transform basis. The random basis choice is achieved by a 50:50 beam splitter. In the computational basis, we directly measure the polarization (H/V) of the photons as well as their arrival time. For the Fourier basis, asymmetric FMIs are needed to perform a projection onto the superposition $(1/\sqrt{2}(|t_0\rangle \pm |t_1\rangle))$ in time-bin DOF after the polarization measurement on $(1/\sqrt{2}(|H\rangle \pm |V\rangle))$. Considering the impact of temperature fluctuations on the phase of the interferometers, we strive to ensure that the fiber lengths are as short as possible when constructing the interferometers, thereby reducing phase disturbances in each arm. Additionally, we isolated the interferometers and maintained phase stability during the measurement process using a phase shifter within the interferometer (see Supplement 1). By adjusting the polarization controller 2 (PC2), we can switch the subspace size between $k = 4$ and $k = 2$. More detailed settings and the corresponding measurement outcomes for each detector click are shown in Section II of Supplement 1. Furthermore, to illustrate the enhancement brought about by high-dimensional systems, we also present an experiment with qubit encoding, i.e., $d = 2$, $k = 2$. In this setting, we only measure the photons in time-bin DOF, and the measurement setup is shown in Supplement 1.

4. ENHANCEMENT IN INFORMATION CAPACITY AND NOISE RESISTANCE

We compare the achievable asymptotic key rate per sifted signal K_{pss} with different dimension settings under varying noise conditions locally. The results are shown in Fig. 2(a). Here, the x-axis represents the amount of classical optical power injected into the fiber. Notably, the noise in this scenario is primarily caused by the imperfect isolation of DWDM, rather than the Raman scattering, which is significantly weaker in short fibers. For the $k = 4$ configuration, it is capable of achieving a greater secure key rate at low noise due to its higher information capacity. When no additional noise is added, we get a secure key rate of 1.34 ± 0.01 bits per sifted signal experimentally, which exceeds the limit of qubit systems. Furthermore, it also exhibits better noise tolerance due to the excellent error tolerance brought by the high information capacity. For the case of $d = 4$, $k = 2$, while it provides lower key rates under low-noise conditions compared to the $k = 4$ configuration, it exhibits greater noise resilience in extreme-noise scenarios. The improved noise resilience primarily comes from the fact that the entanglement of the high-dimensional state is also present in its subspaces, and the smaller coding dimensions also contribute to reducing the error correction cost.

In practical implementation, the performance of high-dimensional systems may deteriorate with the increasing distance due to various disturbances in the channel such as losses, chromatic dispersion, or polarization mode dispersion. To this end, we distribute hyperentangled photons over two different lengths of spooled fiber—2×10 km and 2×25 km, and then evaluate the performance of different dimensional settings. In these scenarios, the noise mainly originates from spontaneous Raman scattering in the fiber channels. The experimental results are shown in Figs. 2(b) and 2(c). As can be seen, the advantages of high-dimensional systems remain. When no extra noise is added, we obtain a secure key rate of more than 1 bit per sifted signal at both 20 km and 50 km distances, with specific values of 1.36 ± 0.02 bits per sifted signal and 1.35 ± 0.02 bits per sifted signal, respectively. Additionally, even after a 50 km distribution and with the injection of up to 47 μW of classical power, at which point noise-induced coincidence events comprise 20% of the total coincidence events, our scheme maintains its capability to generate security keys by encoding information in two-dimensional subspace. This ability to take advantage of high-dimensional entanglement over long distances is aided by the strong robustness of polarization and time-bin DOFs in fiber channels, as well as its convenient subspace dividing and measurement. Compared to the scheme using path entanglement [49], our scheme is more robust in out-of-the-laboratory implementations and can be directly implemented over existing fiber links.

Given the excellent noise resistance of our scheme over long-distance channels, we apply it to the scenario where quantum and classical signals coexist in the same fiber. In this scenario, the classical signal is exceptionally stronger than the quantum signal and can generate noise through various scattering processes [54]. Generally, extra narrow band filters are necessary for such co-transmission applications, but they typically incur additional loss in signal photons. In our experiments, we achieve coexistence with classical signals at different distances without any additional filters. By adjusting the launch power, we ensure that the classical optical power received at each distance is 12 μW, which is sufficient for six 10 Gbps classical communication [54,55]. We measure the key rate in bits per second (bps) to take into account the impact of long-distance fiber loss, and the results are shown in Fig. 3. The intensity of noise here increases linearly with channel length, while the quantum signal decays exponentially (see Supplement 1). Therefore, at a close distance, the high information capacity of the configuration $k = 4$ guarantees a higher achievable key rate, while the excellent noise tolerance of the smaller subspace setting increases the communication distance. Note that, unlike traditional quantum and classical co-propagation experiments, the enhanced performance here arises from the enhancement of the protocol itself brought by high-dimensional entanglement, rather than stringent filtering and other practical strategies. In addition, the high-dimensional scheme is compatible with such practical strategies, presenting a novel solution for this application.

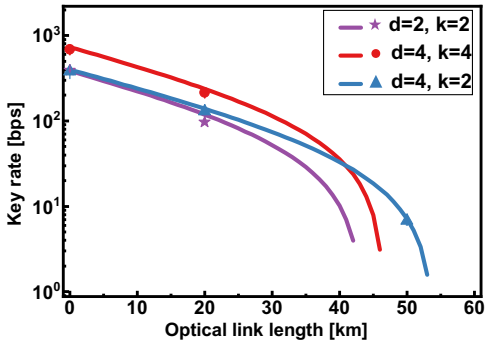

Fig. 3. Secure key rate for co-propagation of QKD and six 10 Gbps classical communication channels over different fiber lengths. The solid lines in the figure are the simulation results, and the discrete points are the experimental results. The error bars are inside the symbols.

5. DISCUSSION AND CONCLUSION

We experimentally demonstrated the enhancement of 4D entanglement on the per-photon information capacity and noise resistance of noisy QKD. In theory, these features can be further amplified through increasing the system dimension. For our system, the dimension can be increased by expanding the time-bin dimension or by multiplexing other degrees of freedom. For the former, the preparation of quantum states can be directly achieved by using a longer pump pulse sequence [42,56]. The main challenge in expanding the time-bin dimension lies in the implementation of superposition measurements, where the construction of complex unbalanced interferometers is required. Fortunately, recent work has demonstrated the feasibility of achieving four-dimensional superposition measurements experimentally [37]. To achieve higher dimensions, more cascades of interferometers are needed. It is currently possible to prepare a large number of interferometers with small arm length difference errors, as demonstrated in some experiments [15,57]. In addition, with the development of space-division multiplexing fiber technology [40], multiplexing other degrees of freedom is also a feasible scheme [58,59]. However, it is also important to exercise caution as increasing the dimensions of the system may also result in increased noise and complexity. There may be an optimal dimension in the experiment, beyond which further increases do not provide additional advantages.

In our experiment, the maximum communication distance achieved is 50 km. Our system is also capable of supporting longer distances, as polarization and time-bin degrees of freedom have

been proven to enable long-distance transmission over fiber channels. For greater distances, dispersion compensation and active polarization stabilization are necessary, and these can be implemented using existing technologies. The primary factor limiting the transmission distance is the poor signal-to-noise ratio at the maximum distance, where the inherent dark count and background noise nearly overwhelm the quantum signal. Therefore, when no additional noise is introduced in the channel, the transmission distance is mainly limited by the dark count rate of the detector. Improving detection efficiency and reducing the number of dark counts can extend the transmission distance. However, when there is significant additional noise in the channel, these two measures will fail, and the maximum achievable distance primarily depends on the noise level. At this point, opting for encoding in a smaller subspace is a wiser choice.

In addition, we notice a time-energy entanglement-based encoding method, which enables flexible dimension settings through discretizing time [36]. Although this method can conveniently achieve ultra-high dimensions without adding experiment complexity, it requires some assumptions about the source, thus compromising the source security. A similar time discretization approach has been employed in recent experiments [50], but it requires the detector to remain active at all time, which may not be desirable in noisy scenarios. Noise can cause the detector to saturate and lead to a high probability of accidental coincidence. In contrast, discrete pulse-pumped systems define the fixed time slots, which can improve the signal-to-noise ratio. Moreover, our scheme can be extended into a trust node-free multi-users quantum communication network through wavelength division multiplexing [13,14].

In quantum key distribution, the security of the final key is also related to the number of signals exchanged between the communication parties. Currently, finite-key analysis of high-dimensional systems has been implemented in some works [31,60]. For the subspace encoding protocol we employed, each subspace can be viewed as a distinct k-dimensional system, so the existing finite-key analysis can be directly used in each subspace. It should be noted that as the number of subspaces increases, the number of signals in each subspace decreases, necessitating the accumulation of more signals. When the number of signals is constrained, the selection of subspace dimensions must also consider the finite-key effects.

In summary, we have experimentally demonstrated a subspace encoding scheme for quantum key distribution in noisy fiber channels. This work also constitutes the longest distance experimental realization of high-dimensional entanglement-based quantum key distribution in fiber channels. By utilizing flexible subspace encoding, we achieved a secure key rate exceeding the qubit limit under low noise. We also established a positive key rate in a state where qubit communication is no longer possible. Furthermore, we demonstrated the benefits of high-dimensional entanglement in both classical and quantum channel multiplexing scenarios by simulating classical signals with additional lasers. It is noteworthy that our scheme is highly practical since it is compatible with existing fiber networks and is ready to be directly adopted for long-distance quantum communication. Additionally, it exhibits source-independent characteristics and can easily be extended to a multi-user quantum network. We believe that this work lays a solid foundation for the practical development of large-scale quantum communication networks, and paves the way for fully exploiting the quantum features of high-dimensional quantum states.

Funding. National Natural Science Foundation of China (62271463, 62301524, 62105318, 61961136004, 62171424); Fundamental Research Funds for the Central Universities; China Postdoctoral Science Foundation (2022M723064); Natural Science Foundation of Anhui Province (2308085QF216); Innovation Program for Quantum Science and Technology (2021ZD0300700).

Acknowledgment. This work was supported by the National Natural Science Foundation of China (Grant No. 62271463, 62301524, 62105318, 61961136004, 62171424), the Fundamental Research Funds for the Central Universities, the China Postdoctoral Science Foundation (Grant No. 2022M723064), Natural Science Foundation of Anhui (No. 2308085QF216), and the Innovation Program for Quantum Science and Technology (Grant No. 2021ZD0300700).

Disclosures. The authors declare no conflicts of interest.

Data availability. Data underlying the results presented in this paper are not publicly available at this time but may be obtained from the authors upon reasonable request.

Supplemental document. See Supplement 1 for supporting content.

REFERENCES

1. C. H. Bennett and G. Brassard, "Quantum cryptography: public key distribution and coin tossing," Theor. Comput. Sci. **560**, 7–11 (2014).
2. A. K. Ekert, "Quantum cryptography based on Bell's theorem," Phys. Rev. Lett. **67**, 661 (1991).
3. C. H. Bennett, G. Brassard, and N. D. Mermin, "Quantum cryptography without Bell's theorem," Phys. Rev. Lett. **68**, 557 (1992).
4. H.-K. Lo and H. F. Chau, "Unconditional security of quantum key distribution over arbitrarily long distances," Science **283**, 2050 (1999).
5. P. W. Shor and J. Preskill, "Simple proof of security of the BB84 quantum key distribution protocol," Phys. Rev. Lett. **85**, 441 (2000).
6. D. Mayers, "Unconditional security in quantum cryptography," J. ACM **48**, 351–406 (2001).
7. F. Xu, X. Ma, Q. Zhang, *et al.*, "Secure quantum key distribution with realistic devices," Rev. Mod. Phys. **92**, 025002 (2020).
8. D. Mayers and A. Yao, "Quantum cryptography with imperfect apparatus," in *Proceedings 39th Annual Symposium on Foundations of Computer Science (Cat. No. 98CB36280)* (IEEE, 1998), pp. 503–509.
9. U. Vazirani and T. Vidick, "Fully device-independent quantum key distribution," Phys. Rev. Lett. **113**, 140501 (2014).
10. W.-Z. Liu, Y.-Z. Zhang, Y.-Z. Zhen, *et al.*, "Toward a photonic demonstration of device-independent quantum key distribution," Phys. Rev. Lett. **129**, 050502 (2022).
11. W. Zhang, T. van Leent, K. Redeker, *et al.*, "A device-independent quantum key distribution system for distant users," Nature **607**, 687–691 (2022).
12. D. P. Nadlinger, P. Drmota, B. C. Nichol, *et al.*, "Experimental quantum key distribution certified by Bell's theorem," Nature **607**, 682–686 (2022).
13. S. Wengerowsky, S. K. Joshi, F. Steinlechner, *et al.*, "An entanglement-based wavelength-multiplexed quantum communication network," Nature **564**, 225–228 (2018).
14. S. K. Joshi, D. Aktas, S. Wengerowsky, *et al.*, "A trusted node-free eight-user metropolitan quantum communication network," Sci. Adv. **6**, eaba0959 (2020).
15. E. Fitzke, L. Bialowons, T. Dolejsky, *et al.*, "Scalable network for simultaneous pairwise quantum key distribution via entanglement-based time-bin coding," PRX Quantum **3**, 020341 (2022).
16. W. Wen, Z. Chen, L. Lu, *et al.*, "Realizing an entanglement-based multiuser quantum network with integrated photonics," Phys. Rev. Appl. **18**, 024059 (2022).
17. G. Ribordy, J. Brendel, J.-D. Gautier, *et al.*, "Long-distance entanglement-based quantum key distribution," Phys. Rev. A **63**, 012309 (2000).
18. I. Marcikic, H. de Riedmatten, W. Tittel, *et al.*, "Distribution of time-bin entangled qubits over 50 km of optical fiber," Phys. Rev. Lett. **93**, 180502 (2004).
19. R. Ursin, F. Tiefenbacher, T. Schmitt-Manderbach, *et al.*, "Entanglement-based quantum communication over 144 km," Nat. Phys. **3**, 481–486 (2007).

20. T. Honjo, S. W. Nam, H. Takesue, *et al.*, "Long-distance entanglement-based quantum key distribution over optical fiber," Opt. Express **16**, 19118–19126 (2008).
21. J. Yin, Y.-H. Li, S.-K. Liao, *et al.*, "Entanglement-based secure quantum cryptography over 1,120 kilometres," Nature **582**, 501–505 (2020).
22. V. Scarani, H. Bechmann-Pasquinucci, N. J. Cerf, *et al.*, "The security of practical quantum key distribution," Rev. Mod. Phys. **81**, 1301 (2009).
23. S. Pirandola, U. L. Andersen, L. Banchi, *et al.*, "Advances in quantum cryptography," Adv. Opt. Photonics **12**, 1012–1017 (2020).
24. K. A. Patel, J. F. Dynes, I. Choi, *et al.*, "Coexistence of high-bit-rate quantum key distribution and data on optical fiber," Phys. Rev. X **2**, 041010 (2012).
25. M. Avesani, L. Calderaro, M. Schiavon, *et al.*, "Full daylight quantum-key-distribution at 1550 nm enabled by integrated silicon photonics," npj Quantum Inf. **7**, 93 (2021).
26. D. Cozzolino, B. Da Lio, D. Bacco, *et al.*, "High-dimensional quantum communication: benefits, progress, and future challenges," Adv. Quantum Technol. **2**, 1900038 (2019).
27. M. Erhard, M. Krenn, and A. Zeilinger, "Advances in high-dimensional quantum entanglement," Nat. Rev. Phys. **2**, 365–381 (2020).
28. H. Bechmann-Pasquinucci and W. Tittel, "Quantum cryptography using larger alphabets," Phys. Rev. A **61**, 062308 (2000).
29. N. J. Cerf, M. Bourennane, A. Karlsson, *et al.*, "Security of quantum key distribution using d-level systems," Phys. Rev. Lett. **88**, 127902 (2002).
30. G. M. Nikolopoulos, K. S. Ranade, and G. Alber, "Error tolerance of two-basis quantum-key-distribution protocols using qudits and two-way classical communication," Phys. Rev. A **73**, 032325 (2006).
31. L. Sheridan and V. Scarani, "Security proof for quantum key distribution using qudit systems," Phys. Rev. A **82**, 030301 (2010).
32. S. Ecker, F. Bouchard, L. Bulla, *et al.*, "Overcoming noise in entanglement distribution," Phys. Rev. X **9**, 041042 (2019).
33. D. Collins, N. Gisin, N. Linden, *et al.*, "Bell inequalities for arbitrarily high-dimensional systems," Phys. Rev. Lett. **88**, 040404 (2002).
34. I. Nape, V. Rodríguez-Fajardo, F. Zhu, *et al.*, "Measuring dimensionality and purity of high-dimensional entangled states," Nat. Commun. **12**, 5159 (2021).
35. F. Zhu, M. Tyler, N. H. Valencia, *et al.*, "Is high-dimensional photonic entanglement robust to noise?" AVS Quantum Sci. **3**, 011401 (2021).
36. T. Zhong, H. Zhou, R. D. Horansky, *et al.*, "Photon-efficient quantum key distribution using time–energy entanglement with high-dimensional encoding," New J. Phys. **17**, 022002 (2015).
37. N. T. Islam, C. C. W. Lim, C. Cahall, *et al.*, "Provably secure and high-rate quantum key distribution with time-bin qudits," Sci. Adv. **3**, e1701491 (2017).
38. D. Cozzolino, D. Bacco, B. Da Lio, *et al.*, "Orbital angular momentum states enabling fiber-based high-dimensional quantum communication," Phys. Rev. Appl. **11**, 064058 (2019).
39. X.-M. Hu, W.-B. Xing, B.-H. Liu, *et al.*, "Efficient generation of high-dimensional entanglement through multipath down-conversion," Phys. Rev. Lett. **125**, 090503 (2020).
40. G. B. Xavier and G. Lima, "Quantum information processing with space-division multiplexing optical fibres," Commun. Phys. **3**, 9 (2020).
41. M. Zahidy, D. Ribezzo, C. De Lazzari, *et al.*, "Practical high-dimensional quantum key distribution protocol over deployed multicore fiber," Nat. Commun. **15**, 1651 (2024).
42. A. Martin, T. Guerreiro, A. Tiranov, *et al.*, "Quantifying photonic high-dimensional entanglement," Phys. Rev. Lett. **118**, 110501 (2017).
43. X.-M. Hu, Y. Guo, B.-H. Liu, *et al.*, "Beating the channel capacity limit for superdense coding with entangled ququarts," Sci. Adv. **4**, eaat9304 (2018).
44. A. Babazadeh, M. Erhard, F. Wang, *et al.*, "High-dimensional single-photon quantum gates: concepts and experiments," Phys. Rev. Lett. **119**, 180510 (2017).
45. H. J. Lee and H. S. Park, "Generation and measurement of arbitrary four-dimensional spatial entanglement between photons in multicore fibers," Photonics Res. **7**, 19–27 (2019).
46. X.-M. Hu, W.-B. Xing, B.-H. Liu, *et al.*, "Efficient distribution of high-dimensional entanglement through 11 km fiber," Optica **7**, 738–743 (2020).
47. H. Cao, S.-C. Gao, C. Zhang, *et al.*, "Distribution of high-dimensional orbital angular momentum entanglement over a 1 km few-mode fiber," Optica **7**, 232–237 (2020).
48. M. Doda, M. Huber, G. Murta, *et al.*, "Quantum key distribution overcoming extreme noise: Simultaneous subspace coding using high-dimensional entanglement," Phys. Rev. Appl. **15**, 034003 (2021).
49. X.-M. Hu, C. Zhang, Y. Guo, *et al.*, "Pathways for entanglement-based quantum communication in the face of high noise," Phys. Rev. Lett. **127**, 110505 (2021).
50. L. Bulla, M. Pivoluska, K. Hjorth, *et al.*, "Nonlocal temporal interferometry for highly resilient free-space quantum communication," Phys. Rev. X **13**, 021001 (2023).
51. B.-X. Wang, Y. Mao, L. Shen, *et al.*, "Long-distance transmission of quantum key distribution coexisting with classical optical communication over a weakly-coupled few-mode fiber," Opt. Express **28**, 12558–12565 (2020).
52. T. Kim, M. Fiorentino, and F. N. C. Wong, "Phase-stable source of polarization-entangled photons using a polarization Sagnac interferometer," Phys. Rev. A **73**, 012316 (2006).
53. A. Fedrizzi, T. Herbst, A. Poppe, *et al.*, "A wavelength-tunable fiber-coupled source of narrowband entangled photons," Opt. Express **15**, 15377–15386 (2007).
54. R. Valivarthi, P. Umesh, C. John, *et al.*, "Measurement-device-independent quantum key distribution coexisting with classical communication," Quantum Sci. Technol. **4**, 045002 (2019).
55. K. Patel, J. Dynes, M. Lucamarini, *et al.*, "Quantum key distribution for 10 Gb/s dense wavelength division multiplexing networks," Appl. Phys. Lett. **104**, 051123 (2014).
56. H. de Riedmatten, I. Marcikic, V. Scarani, *et al.*, "Tailoring photonic entanglement in high-dimensional Hilbert spaces," Phys. Rev. A **69**, 050304 (2004).
57. S. Wang, W. Chen, Z.-Q. Yin, *et al.*, "Field and long-term demonstration of a wide area quantum key distribution network," Opt. Express **22**, 21739–21756 (2014).
58. Z. Xie, T. Zhong, S. Shrestha, *et al.*, "Harnessing high-dimensional hyperentanglement through a biphoton frequency comb," Nat. Photonics **9**, 536–542 (2015).
59. L. Achatz, L. Bulla, S. Ecker, *et al.*, "Simultaneous transmission of hyper-entanglement in three degrees of freedom through a multicore fiber," npj Quantum Inf. **9**, 45 (2023).
60. R. Wang, Z.-Q. Yin, H. Liu, *et al.*, "Tight finite-key analysis for generalized high-dimensional quantum key distribution," Phys. Rev. Res. **3**, 023019 (2021).